JOURNAL OF COMPUTATIONAL PHYSICS **125,** 454–463 (1996)
ARTICLE NO. 0107

# An Efficient Method for Temporal Integration of the Navier–Stokes Equations in Confined Axisymmetric Geometries

KNUT AKSELVOLL AND PARVIZ MOIN

*Department of Mechanical Engineering, Stanford University, Stanford, California 94305*

Received March 9, 1995; revised September 26, 1995

A method for temporal integration of the Navier–Stokes equations written in cylindrical coordinates is described. The objective is to avoid the severe time-step limitation usually encountered in confined axisymmetric geometries (e.g., pipe flow), caused by a fine azimuthal grid spacing around the centerline and the desire to refine the grid in the radial direction near walls. Avoiding severe time-step limitations usually involves treating all terms with derivatives in the radial and azimuthal directions with an implicit time-integration scheme. However, this leads to a set of coupled nonlinear equations which generally require complex and costly solution procedures. The scheme described in this paper decomposes the computational domain into two regions. Within each region only the derivatives in one coordinate direction is treated implicitly. Conditions at the interface between the regions are determined to maintain the overall temporal accuracy of the basic time-integration schemes. Results from a direct numerical simulation (DNS) of turbulent pipe flow are validated against computational and experimental results from the literature. It is demonstrated that this new scheme allows for larger time-steps than other schemes, leading to significant CPU savings. 

## 1. INTRODUCTION

This paper describes a method developed for temporal integration of the unsteady, incompressible, Navier–Stokes equations written in cylindrical coordinates. There are two main problems associated with solving the Navier–Stokes equations in cylindrical (or spherical) coordinates. The first is related to the treatment of the coordinate singularity at the centerline ($r = 0$). Solutions to this problem are described in the literature (e.g., [1–4]) and are not included in this paper.

A second, and equally important, problem is related to the fact that when using cylindrical coordinates the azimuthal grid resolution is proportional to the radial distance from the centerline. For confined axisymmetric *turbulent* flows (e.g., pipe flow) the azimuthal grid resolution requirement is usually dictated by the resolution of the near wall coherent structures of the flow. This leads to a significant overresolution in the azimuthal direction around the centerline which leads to severe time-step limitations if explicit time-integration schemes are used.

One technique that has been used in the past in order to overcome the time-stepping (or the pole) problem, involves coarsening the grid near the singular points, thus allowing for the use of explicit time-integration. For instance, Kurihara [5] developed what he called a spherical grid system in order to reduce the grid spacing close to the poles in a simulation of the general circulation of the atmosphere. Umsheid and Sankar-Rao [6], also interested in the general circulation problem, filtered the small scale portion of the solution near the poles. Filtering was done either in physical space or in the Fourier space. This effectively coarsens the grid near the poles, thus allowing for larger time-steps.

In some axisymmetric cases the problem has been addressed by treating all terms (both convective and diffusive) with derivatives in the azimuthal direction implicitly (e.g., [2, 7]). However, the drawback of this approach is the time-step restriction due to radial refinement of the mesh near walls. One remedy would be to treat all terms with derivatives in both the radial and azimuthal directions implicitly. This procedure gives a set of nonlinear coupled equations which usually require complicated and costly solution algorithms (often involving iterations or approximate factorization techniques).

The need to treat the convective terms (with derivative in the azimuthal direction) implicitly near the centerline arises because the azimuthal velocity component is usually significant in the core region of the pipe. The more traditional approach of treating all the diffusive terms implicitly and all the convective terms explicitly (see [8]) is based on the assumption that the grid is fine only near walls, where the wall-normal velocity is very small. In such cases the convective terms are usually not important in terms of limiting the time-step. However, in any situation where the grid is fine in a region with significant convection velocities, implicit treatment of the convective terms would have to be considered. (See [1] for other examples of such flows.)

The method described in this paper is based on the realization that in the central region of the flow (i.e., a region enclosing the centerline) terms with derivatives in the azimuthal direction will be the most restrictive in terms of limiting the time-step. Both the axial and radial grid



0021-9991/96 $18.00

spacings are usually large in this region and the simpler explicit time-integration schemes can be used on terms with derivatives in these directions. At the wall (of a pipe) the radial grid spacing is usually significantly finer than both the axial and azimuthal grid spacings, meaning that only terms with derivatives in the radial direction (in most cases only the diffusive terms) need to be treated with implicit time-integrations schemes.

The basic idea behind the method is to divide the computational domain into two separate regions. One is denoted the ''core region'' and extends from the centerline to some radius $r_c$, i.e., $0 < r < r_c$. In this region all the terms in the momentum equations with derivatives in the azimuthal direction are treated implicitly. (Note that because large azimuthal convection velocities are expected around the centerline, convective as well as diffusive terms will have to be treated implicitly). All other terms are treated explicitly. The second region is denoted the ''outer region'' and consists of the remaining part of the domain, i.e. $r_c < r < R$, where $R$ is the radius of the pipe. (This region includes a solid wall, perpendicular to the radial direction). In this region the diffusive terms, and in some cases also the convective terms (see [1]), with derivatives in the radial direction, are treated implicitly. All other terms are treated explicitly. Conditions at the interface between the two regions are determined such that the overall temporal accuracy of the basic time-integration scheme is conserved.

The use of semi-implicit schemes in the calculation of flows in geometries that have singular points does not in itself represent a new idea. For instance, Oberhuber [9] used the semi-implicit method proposed by Kwizak and Robert [10] in a simulation of the Atlantic circulation. Eggels *et al.* [2] and Wagner and Friedrich [7] employed a semi-implicit scheme to integrate the Navier–Stokes equations in axisymmetric geometries. The new feature of the method described in this paper is a temporal decomposition of the computational domain. The computational domain is decomposed in order to avoid having a fine grid spacing in more than one direction within each of the regions. This gives the flexibility of using different time-integration schemes in different parts of the computational domain and allows for implicit treatment of only one coordinate direction which greatly simplifies the solution procedure as well as reduces computational time.

The proposed method is validated by applying it to direct numerical simulation (DNS) of turbulent flow in a circular pipe. However, the method has potentially a wider range of applications, particularly in fundamental turbulence simulations. For instance, Akselvoll and Moin [1] used the present method to calculate mixing of turbulent confined coannular jets. The method allowed for a significant increase in time-step compared with other more traditional methods. Other applications are calculations of diffusers, jets, vortex rings, etc. The utility of temporal decomposition is not limited to cylinderical or spherical geometries, it has potential applications in computations of flows in complex geometries where the grid is refined in several separate regions.

## 2. GOVERNING EQUATIONS

The governing equations are the incompressible Navier–Stokes and continuity equations. Body forces have been neglected and the viscosity is assumed to be a function of space (in order to account for simple turbulence models). These equations can be written in vector form as

$$\frac{\partial \mathbf{u}}{\partial t} = -\nabla p + \nabla \cdot \mathbf{s}, \tag{1}$$

$$\nabla \cdot \mathbf{u} = 0, \tag{2}$$

where $\mathbf{u}$ is the velocity vector and $\mathbf{s}$ is a symmetric tensor given by

$$\mathbf{s} = \nu \nabla \mathbf{u} + \nu (\nabla \mathbf{u})^{\mathrm{T}} - \mathbf{u} \otimes \mathbf{u}. \tag{3}$$

The components of $\mathbf{s}$ are (in cylindrical coordinates)

$$\begin{aligned}
s_{xx} &= 2\nu \frac{\partial u_x}{\partial x} - u_x u_x, \\
s_{\theta\theta} &= 2\nu \left( \frac{1}{r} \frac{\partial u_\theta}{\partial \theta} + \frac{u_r}{r} \right) - u_\theta u_\theta, \\
s_{r\theta} &= \nu \left( \frac{\partial u_\theta}{\partial r} + \frac{1}{r} \frac{\partial u_r}{\partial \theta} - \frac{u_\theta}{r} \right) - u_r u_\theta, \\
s_{rr} &= 2\nu \frac{\partial u_r}{\partial r} - u_r u_r, \\
s_{xr} &= \nu \left( \frac{\partial u_r}{\partial x} + \frac{\partial u_x}{\partial r} \right) - u_x u_r, \\
s_{x\theta} &= \nu \left( \frac{\partial u_\theta}{\partial x} + \frac{1}{r} \frac{\partial u_x}{\partial \theta} \right) - u_x u_\theta.
\end{aligned} \tag{4}$$

In this paper $x$, $r$, and $\theta$ are used to denote the axial, radial, and azimuthal directions, respectively; $\nu$ is the total viscosity which in DNS is equal to the molecular viscosity and in large eddy simulation (LES) is equal to the sum of the molecular and eddy-viscosity; $u_x$, $u_r$, and $u_\theta$ are the components of the velocity vector in the axial, radial, and azimuthal directions, respectively.

## 3. TEMPORAL INTEGRATION SCHEME

The principle of decomposing the computational domain into two regions can be used with any combination of

explicit/implicit time-integration schemes. However, for the purpose of the present illustrations a three-step predictor–corrector algorithm of the Runge–Kutta genre is used [11, 12]. This is a hybrid scheme essentially using RK3 (third-order accurate) for the explicitly treated terms and Crank–Nicolson (second order accurate) for the implicitly treated terms. The three-step time-advancement scheme for the Navier–Stokes and continuity equations can be written

$$\frac{u_i^q - u_i^{q-1}}{\Delta t} = -2\beta_q G_i(p^q) + \beta_q\{B_i^q + B_i^{q-1}\} + \gamma_q A_i^{q-1} + \zeta_q A_i^{q-2}, \quad (5)$$

$$D_i(u_i^q) = 0, \quad (6)$$

where $A$ and $B$ are operators acting on the velocity vector, and subscript $i$ represents $x$, $r$, or $\theta$. $A$ includes terms treated explicitly and $B$ includes terms treated implicitly. $G$ is the gradient operator and $D$ is the divergence operator. Superscript $q$ ($q = 1, 2, 3$) represents the Runge–Kutta substeps such that $u^{q-1} = u^n$ for $q = 1$ and $u^q = u^{n+1}$ for $q = 3$. (Note that $\zeta_q = 0$ for $q = 1$). Superscript $n$ represents the full time-step. The coefficients, $\beta_q$, $\gamma_q$, and $\zeta_q$ are selected such that the total time advancement is third-order accurate for the explicitly treated terms and second-order accurate for the implicitly treated terms. These coefficients are

$$\beta_1 = \tfrac{4}{15}, \quad \beta_2 = \tfrac{1}{15}, \quad \beta_3 = \tfrac{1}{6},$$
$$\gamma_1 = \tfrac{8}{15}, \quad \gamma_2 = \tfrac{5}{12}, \quad \gamma_3 = \tfrac{3}{4},$$
$$\zeta_1 = 0, \quad \zeta_2 = -\tfrac{17}{60}, \quad \zeta_3 = -\tfrac{5}{12},$$
$$\sum_{q=1}^{3} 2\beta_q = \sum_{q=1}^{3} (\gamma_q + \zeta_q) = 1.$$

For further details of this hybrid time-integration scheme the reader is referred to Refs. [1, 11, or 12].

In the present calculations, the standard fractional step method is used to remove the implicit pressure dependence in Eq. (5) and to enforce the equation of continuity. The reader is referred to [1, 8, 13, or 14] for this and other versions of the fractional step method.

## 4. DOMAIN DECOMPOSITION

The spatial discretization scheme used in the present calculations is based on the second-order finite volume formulation. The governing equations are solved on a staggered grid [15]. The computational domain is divided into two separate regions in which different terms of the Navier–Stokes equations are grouped into the explicit and implicit operators, $A$ and $B$. The cross section of the two regions are illustrated in Fig. 1.

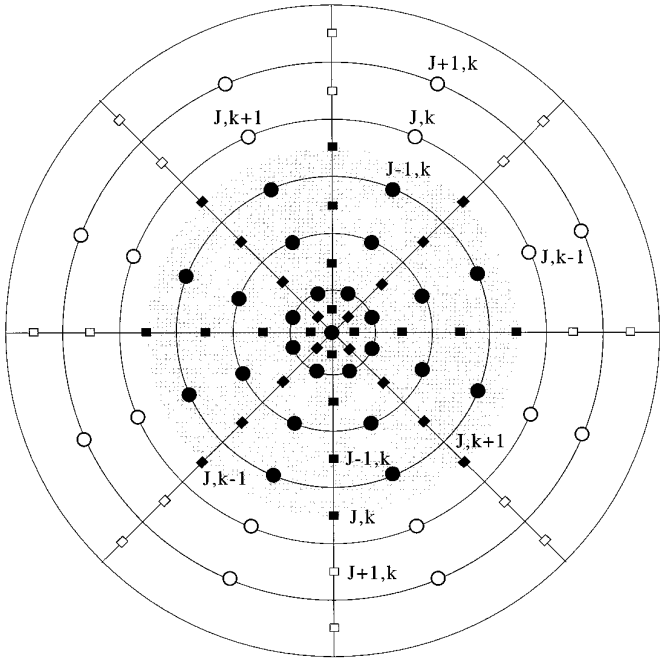


**FIG. 1.** Computational domain and the staggered mesh system. The shaded area represents the core region which is surrounded by the outer region: ○ and □ are locations where $u_r$ and $u_\theta$ are defined, respectively.

Due to the fine azimuthal grid spacing in the near centerline region it is desirable to treat all terms (convective and diffusive) with derivatives in the azimuthal direction implicitly in the core region. (This will become apparent in Section 8). The operators $A$ and $B$ therefore become

$$A_x = \frac{\partial s_{xx}}{\partial x} + \frac{1}{r}\frac{\partial r s_{xr}}{\partial r} + \frac{1}{r}\frac{\partial}{\partial \theta}\left(\nu \frac{\partial u_\theta}{\partial x}\right). \quad (7a)$$

$$A_r = \frac{\partial s_{rx}}{\partial x} + \frac{1}{r}\frac{\partial r s_{rr}}{\partial r} + \frac{1}{r}\frac{\partial}{\partial \theta}\left(\nu \frac{\partial u_\theta}{\partial r} - \nu \frac{u_\theta}{r}\right) - \frac{s_{\theta\theta}}{r}. \quad (7b)$$

$$A_\theta = \frac{\partial s_{\theta x}}{\partial x} + \frac{1}{r}\frac{\partial r s_{\theta r}}{\partial r} + \frac{1}{r}\frac{\partial}{\partial \theta}\left(\frac{2\nu u_r}{r}\right) + \frac{s_{\theta r}}{r}. \quad (7c)$$

$$B_x = \frac{1}{r}\frac{\partial}{\partial \theta}\left(\frac{\nu}{r}\frac{\partial u_x}{\partial \theta}\right) - \frac{1}{r}\frac{\partial u_x u_\theta}{\partial \theta}. \quad (8a)$$

$$B_r = \frac{1}{r}\frac{\partial}{\partial \theta}\left(\frac{\nu}{r}\frac{\partial u_r}{\partial \theta}\right) - \frac{1}{r}\frac{\partial u_r u_\theta}{\partial \theta}. \quad (8b)$$

$$B_\theta = \frac{1}{r}\frac{\partial}{\partial \theta}\left(2\frac{\nu}{r}\frac{\partial u_\theta}{\partial \theta}\right) - \frac{1}{r}\frac{\partial u_\theta u_\theta}{\partial \theta}. \quad (8c)$$

From Eq. (8c) it is apparent that the azimuthal momentum equation is non-linear (in $u_\theta$). However, the axial and radial momentum equations are linear in $u_x$ and $u_r$, respectively, although they will require $u_\theta^q$ in order to calculate the coefficients in the tridiagonal matrices (see the next section). The azimuthal momentum equation, on the other hand, is uncoupled from the two other equations. The solution procedure therefore involves linearizing the azimuthal momentum equation (retaining second-order accuracy) and solving it first. The axial and radial momentum equations can then be solved.

Implicit treatment of diffusive and convective terms with derivatives in only one coordinate direction leads to only one nonlinear equation. This means that only one of the convective terms in one of the momentum equations has to be linearized, after which the entire set of equations can easily be solved. In contrast, if convective terms in more than one coordinate direction were treated implicitly the result would be a coupled set of nonlinear equations requiring a significantly more complex solution procedure.

Note that cross-terms (i.e., diffusive terms with mixed derivatives, which are present because of a nonuniform viscosity) are all treated explicitly, despite the fact that some contain azimuthal derivatives. The justification for doing this is that $\Delta x$ and $\Delta r$ are much larger than $r\Delta\theta$ around the centerline, and the cross-terms are therefore not nearly as important as the diffusive terms (already treated implicitly) in terms of causing time-step limitations. However, they may in some cases be important compared with convective terms, particularly if there are large spatial gradients in the viscosity, although this has not been the case in any of the calculations performed by the authors (see [1]).

The solution procedure in the outer region is identical to that in the core region except that all terms with derivatives in the radial direction are treated implicitly. (For flow in a pipe it is not necessary to treat the non-linear term implicitly; however, it may be important in other geometries as shown in [1]). The $A$ and $B$ operators in the outer region become

$$A_x = \frac{\partial s_{xx}}{\partial x} + \frac{1}{r}\frac{\partial}{\partial r}\left(r\nu\frac{\partial u_r}{\partial x}\right) + \frac{1}{r}\frac{\partial s_{x\theta}}{\partial \theta}. \tag{9a}$$

$$A_r = \frac{\partial s_{rx}}{\partial x} + \frac{1}{r}\frac{\partial s_{r\theta}}{\partial \theta} - \frac{s_{\theta\theta}}{r}. \tag{9b}$$

$$A_\theta = \frac{\partial s_{\theta x}}{\partial x} + \frac{1}{r}\frac{\partial}{\partial r}\left(\nu\frac{\partial u_r}{\partial \theta} - \nu u_\theta\right) + \frac{1}{r}\frac{\partial s_{\theta\theta}}{\partial \theta} + \frac{s_{r\theta}}{r}. \tag{9c}$$

$$B_x = \frac{1}{r}\frac{\partial}{\partial r}\left(r\nu\frac{\partial u_x}{\partial r}\right) - \frac{1}{r}\frac{\partial (ru_x u_r)}{\partial r}. \tag{10a}$$

$$B_r = \frac{1}{r}\frac{\partial}{\partial r}\left(2r\nu\frac{\partial u_r}{\partial r}\right) - \frac{1}{r}\frac{\partial (ru_r u_r)}{\partial r}. \tag{10b}$$

$$B_\theta = \frac{1}{r}\frac{\partial}{\partial r}\left(r\nu\frac{\partial u_\theta}{\partial r}\right) - \frac{1}{r}\frac{\partial (ru_\theta u_r)}{\partial r}. \tag{10c}$$

In this region, the radial momentum equation is nonlinear and has to be linearized. This equation must then be solved prior to solving the axial and azimuthal momentum equations since the two latter equations require $u_r^q$ in order to calculate the coefficients in the tridiagonal matrices.

## 5. TREATMENT AT THE INTERFACE

The first step of the solution procedure involves integrating the momentum equations in the core region. For the axial and azimuthal momentum equations, integration includes all points marked by solid symbols (Fig. 1), up to and including the points with radial index $j = J$. The radial momentum equation, on the other hand, can only be integrated up to and including points with radial index $j = J - 1$, as seen by studying the coefficients $a_q$, $b_q$, and $c_q$ in Eq. (11b). Equation (11) shows the general form of the discrete momentum equations in the core region using Eqs. (7) and (8) for the $A$ and $B$ operators. The coefficients $a_q$, $b_q$, and $c_q$ are the elements of the diagonals of the tridiagonal matrix formed on the left-hand side of the equations.

The axial momentum equation ($j \le J$) is

$$a_q u^q_{i,j,k-1} + b_q u^q_{i,j,k} + c_q u^q_{i,j,k+1} = \mathrm{RHS}^{q-1}_{i,j,k}, \tag{11a}$$

where the functional dependence of the coefficients are

$$a_q = a_q(w^q_{i+1,j,k-1}, w^q_{i,j,k-1}),$$
$$b_q = b_q(w^q_{i+1,j,k-1}, w^q_{i,j,k-1}, w^q_{i+1,j,k}, w^q_{i,j,k}),$$
$$c_q = c_q(w^q_{i+1,j,k}, w^q_{i,j,k}).$$

The radial momentum equation ($j \le J - 1$) is

$$a_q v^q_{i,j,k-1}, + b_q v^q_{i,j,k} + c_q v^q_{i,j,k+1} = \mathrm{RHS}^{q-1}_{i,j,k}, \tag{11b}$$

where

$$a_q = a_q(w^q_{i,j+1,k-1}, w^q_{i,j,k-1})$$
$$b_q = b_q(w^q_{i,j+1,k-1}, w^q_{i,j,k-1}, w^q_{i,j+1,k}, w^q_{i,j,k}),$$
$$c_q = c_q(w^q_{i,j+1,k}, w^q_{i,j,k}).$$

The azimuthal momentum equation ($j \le J$) can be written as

$$a_q = w^q_{i,j,k-1} + b_q w^q_{i,j,k} + c_q w^q_{i,j,k+1} = \mathrm{RHS}^{q-1}_{i,j,k}, \quad (11c)$$

where

$$a_q = a_q(w^{q-1}_{i,j,k-1}, w^{q-1}_{i,j,k}),$$
$$b_q = b_q(w^{q-1}_{i,j,k-1}, w^{q-1}_{i,j,k+1}),$$
$$c_q = c_q(w^{q-1}_{i,j,k+1}, w^{q-1}_{i,j,k}).$$

Here, $u$, $v$, and $w$ have been used to denote the axial, radial, and azimuthal velocity components, respectively. The subscripts $(i, j, k)$ give the nodal position at which the velocity components and the right-hand side, RHS, are evaluated. The right-hand side contains only known information (i.e., from substep $q - 1$).

As explained in the previous section the azimuthal momentum equation has to be inverted first. Equation (11c) shows that the coefficients, $a_q$, $b_q$, and $c_q$, only depend on information from the previous substep $(q - 1)$ (due to linearization) and the azimuthal momentum equation can therefore be integrated up to and including points with radial coordinate $j = J$. It is further seen that evaluation of $a_q$, $b_q$, and $c_q$ for the axial momentum equation will require $w^q$ up to and including radial location $j = J$, which is now available.

The ''problem'' arises in the radial momentum equation, where it is seen from Eq. (11b) that the coefficients $a_q$, $b_q$, and $c_q$, depend on $u^q_\theta$ up to and including radial location $j + 1$. The radial momentum equation can therefore only be solved at points with radial location up to and including $j = J - 1$ (in the core region).

The outer region contains all points not included in the core region. Thus the axial and azimuthal momentum equations are integrated from $j = J + 1$ to the wall and the radial momentum equation is integrated from $j = J$ to the wall. Since all terms with derivatives in the radial direction are treated implicitly in the outer region, the general form of the discrete momentum equations in this region become:

The axial momentum equation $(j \geq J + 1)$,

$$a_j u^q_{i,j-1,k} + b_j u^q_{i,j,k} + c_j u^q_{i,j+1,k} = \mathrm{RHS}^{q-1}_{i,j,k}, \quad (12a)$$

where

$$a_j = a_j(v^q_{i+1,j-1,k}, v^q_{i,j-1,k}),$$
$$b_j = b_j(v^q_{i+1,j-1,k}, v^q_{i,j-1,k}, v^q_{i+1,j,k}, v^q_{i,j,k}),$$
$$c_j = c_j(v^q_{i+1,j,k}, v^q_{i,j,k}).$$

The radial momentum equation $(j \geq J)$,

$$a_j v^q_{i,j-1,k} + b_j v^q_{i,j,k} + c_j v^q_{i,j+1,k} = \mathrm{RHS}^{q-1}_{i,j,k}, \quad (12b)$$

where

$$a_j = a_j(v^{q-1}_{i,j-1,k}, v^{q-1}_{i,j,k}),$$
$$b_j = b_j(v^{q-1}_{i,j-1,k}, v^{q-1}_{i,j,k}, v^{q-1}_{i,j+1,k}),$$
$$c_j = c_j(v^{q-1}_{i,j+1,k}, v^{q-1}_{i,j,k}).$$

The azimuthal momentum equation $(j \geq J + 1)$,

$$a_j w^q_{i,j-1,k} + b_j w^q_{i,j,k} + c_j w^q_{i,j+1,k} = \mathrm{RHS}^{q-1}_{i,j,k}, \quad (12c)$$

where

$$a_j = a_j(v^q_{i,j-1,k+1}, v^q_{i,j-1,k}),$$
$$b_j = b_j(v^q_{i,j-1,k+1}, v^q_{i,j-1,k}, v^q_{i,j,k+1}, v^q_{i,j,k}),$$
$$c_j = c_j(v^q_{i,j,k+1}, v^q_{i,j,k}).$$

In this case the radial momentum equation (12b) will have to solved first to yield $v^q$. After solving Equation (12b), $v^q$ is known in the entire domain and the coefficients $a_q$, $b_q$, and $c_q$ in the two other momentum equations can easily be solved.

Solution of Eqs. (12) will, however, require some boundary condition at $j = J$ (axial and azimuthal momentum equations) and $j = J - 1$ (radial momentum equation). But, since Eqs. (11) have been solved first, $u^q$, $v^q$, and $w^q$ are already known at their respective boundaries ($j = J$ for $u$ and $w$ and $j = J - 1$ for $v$) and can be used as boundary conditions when solving Eqs. (12). It is easily verified that this preserves second-order temporal accuracy.

## 6. VERIFICATION OF TEMPORAL ACCURACY

In order to verify the order of accuracy of the scheme a numerical experiment was conducted using turbulent flow in a pipe as a test case. The parameters were the same as for the simulation described in the next section, with the exception of the grid resolution which was only $32 \times 38 \times 64$ (axial, radial, and azimuthal directions). Even though this resolution is insufficient to yield an accurate DNS solution, it is sufficient for the purpose of evaluating the temporal error of the numerical scheme.

Several calculations were performed starting from a fully developed flow field at time $T_1$, advancing to time $T_2$. The number of time-steps used to cover the given time interval was increased from 1 to 1000. The solution obtained using the smallest $\Delta t$ was interpreted as the ''exact solution.'' The error in the solutions obtained at increasing $\Delta t$ was formed by calculating the rms of the difference in the solution obtained at a given $\Delta t$ when compared with the

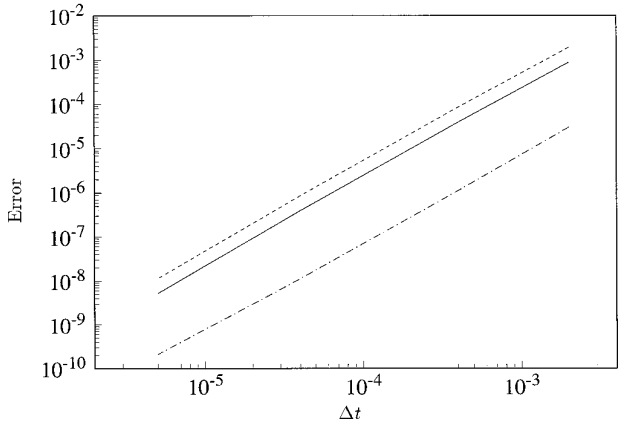


**FIG. 2.** Error in temporal integration scheme: ———, entire domain; ---, core region; –·–, outer region.

"exact solution." In addition to calculating an average error over the entire computational domain, separate error estimates were obtained in the core and outer regions.

A result from these calculations is shown in Fig. 2, using the error in the axial velocity component as example. The slope of the curves (in log–log coordinates) is 2, which verifies that the velocity field is calculated to second-order accuracy. (Similar results were obtained from evaluating the error in the other two velocity components).

In order to show that second-order accuracy is conserved at the interface between the core and the outer region, the error was calculated separately at the grid-points located adjacent to the interface, both in the core and the outer regions. Figure 3 shows these results (again using the error in the axial velocity component as an example). It is apparent that the solution is second-order accurate everywhere.

The code used for the turbulent pipe flow calculations treated only the diffusive terms in the radial direction in the outer region with the second-order implicit Crank–Nicolson scheme. All other terms were treated with the third-order explicit RK3 scheme. In the core region both diffusive and convective terms with derivatives in the azimuthal direction were treated with the second-order Crank–Nicolson scheme. Because the RK3 scheme is third order, the contribution to the total error from the terms treated with this scheme is smaller than the error from the terms treated with the second-order Crank–Nicolson scheme. Thus, the (temporal) error is dominated by the terms treated implicitly. Since two terms, one of which is linearized, are treated with the implicit scheme in the core region versus only one term in the outer region, it is expected that the error is larger in the core region. This explains why the error in the solution is less in the outer region than in the core region. However, the fact remains that scheme is overall second-order accurate.

## 7. DNS OF TURBULENT PIPE FLOW

The numerical scheme outlined above was developed for a code used to study turbulent mixing in a coaxial jet-combustor [1]. Prior to performing the calculation of the coaxial jet-combustor, the numerical scheme was tested extensively in turbulent flow in a pipe (using both large eddy simulation, LES, and direct numerical simulation, DNS). This section presents results from the DNS.

The computational domain consists of a pipe with radius $R$ and length $10R$. The Reynolds number was 180 based on pipe radius, $R$, and friction velocity, $u_\tau$. Periodic boundary conditions were used in the axial and azimuthal directions, and no-slip was used at the wall. The computational grid was stretched in the radial direction and uniform in the axial and azimuthal directions. The grid contained $256 \times 68 \times 128$ points in the axial, radial, and azimuthal directions, respectively. The calculation was run at a time-step, $\Delta t = 0.001R/u_\tau$. The boundary between the core region and outer region was located at $r_c = 0.5R$. (See Section 9 for an explanation of the choice of $r_c$.)

Results from this calculation are compared with computational results obtained by Eggels *et al.* [2] and experimental results obtained by Westerweel *et al.* [16]. Both studies used $Re_\tau = 180$. The computational domain used in [2] was the same as that used in the present study. Eggels *et al.* [2], however, treated all terms with derivatives in the azimuthal direction implicitly in the entire computational domain. Their time-step was therefore limited by the radial resolution requirement at the wall. The grid contained $256 \times 96 \times 128$ points in the axial, radial, and azimuthal directions, respectively. Uniform distribution was used in all coordinate directions. Numerical stability considerations limited the maximum time-step to $0.0004\ R/u_\tau$. This is 2.5 times smaller than that used in the present calculation.

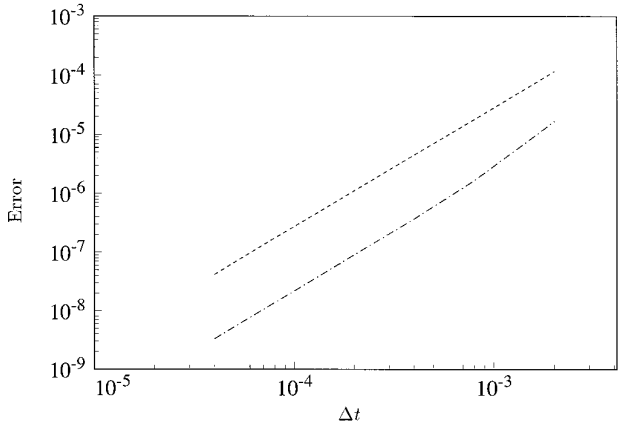


**FIG. 3.** Error in temporal integration scheme at the interface: ---, at $r_c$ in the core region; –·–, at $r_c$ in the outer region.

**TABLE I**

Grid Resolution in Wall Coordinates

| | DNS-AM | DNS-E |
|---|---|---|
| $\Delta x^+$ | 7.03 | 7.03 |
| $(R\ \Delta\theta)^+$ | 8.84 | 8.84 |
| $(\Delta r\ \Delta\theta)^+_{\mathrm{cl}}$ | 0.13 | 0.09 |
| $\Delta r^+_{\mathrm{wall}}$ | 0.17 | 1.88 |
| $\Delta r^+_{\mathrm{max}}$ | 5.94 | 1.88 |

*Note.* DNS-AM is the present DNS results, and DNS-E is the DNS of Eggels *et al.* [2].

The grid resolution in wall-coordinates for the two cases is listed in Table I.

The calculation was started from an initial field of random numbers and run to a statistically steady state before sampling statistics. Statistics were sampled by averaging over the homogenous directions (axial and azimuthal) and time.

Figure 4 shows an instantaneous snapshot of the axial velocity component in an $r - \theta$ plane, and Fig. 5 shows an instantaneous snapshot of the streamwise vorticity in the same plane. Notice that the contours show no trace of the interface between the core and the outer region.

Several mean-flow properties from the present simulation and the reference cases are listed in Table II.

Following Eggels *et al.* [2], the following definitions were adopted for the displacement thickness, $\delta^*$, and the momentum thickness, $\theta^*$,

$$\delta^*(2-\delta^*) = 2\int_0^1 r\left(1-\frac{u_x(r)}{U_{\mathrm{cl}}}\right)dr, \tag{13}$$

$$\theta^*(2-\theta^*) = 2\int_0^1 r\frac{u_x(r)}{U_{\mathrm{cl}}}\left(1-\frac{u_x(r)}{U_{\mathrm{cl}}}\right)dr, \tag{14}$$

where $U_{\mathrm{cl}}$ is the centerline velocity and all variables have been normalized using the radius, $R$, and the friction velocity, $u_\tau$. The coefficient of friction given in Table II is based

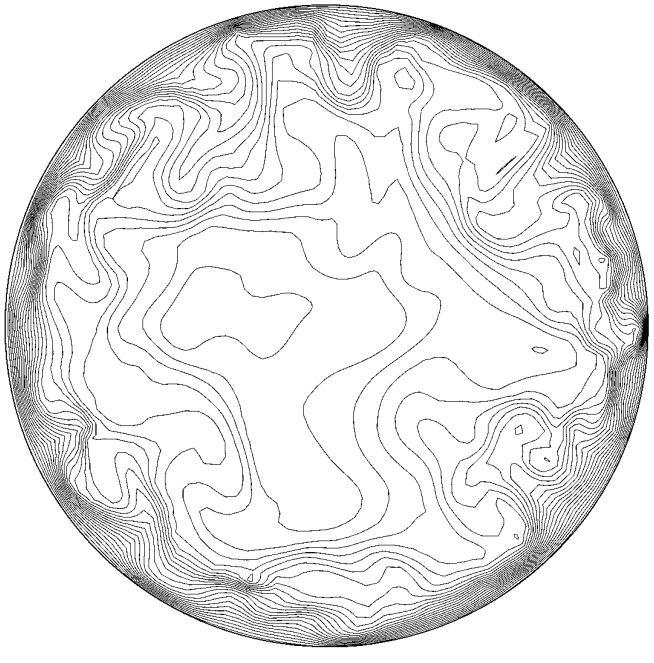

**FIG. 4.** Instantaneous contours of the axial velocity component in a $r-\theta$ plane.

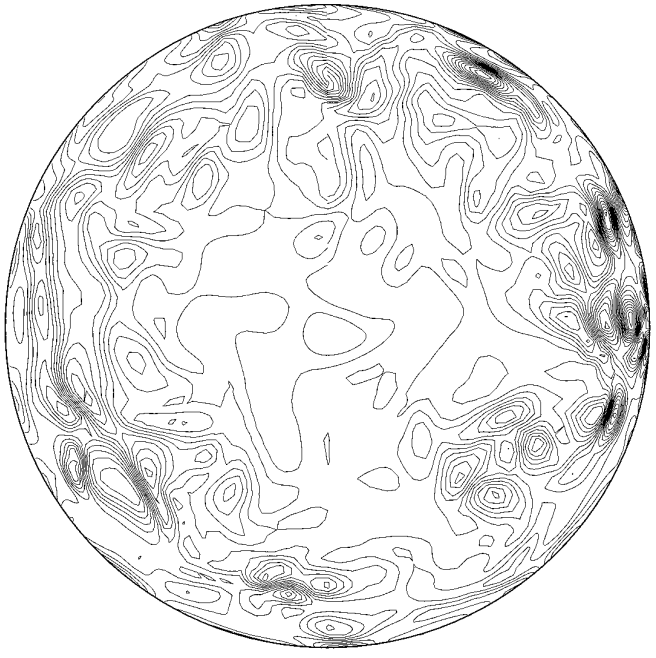

**FIG. 5.** Instantaneous contours of the axial vorticity in a $r-\theta$ plane.

**TABLE II**

Mean Flow Properties

| | DNS-AM | DNS-E | PIV | LDA |
|---|---|---|---|---|
| $Re_\tau$ | 180 | 180 | 183 | 185.5 |
| $U_{\mathrm{cl}}$ | 19.32 | 19.31 | 19.38 | 19.39 |
| $U_{\mathrm{b}}$ | 14.70 | 14.73 | 14.88 | 14.68 |
| $U_{\mathrm{cl}}/U_{\mathrm{b}}$ | 1.31 | 1.31 | 1.30 | 1.32 |
| $C_f \times 10^3$ | 9.25 | 9.22 | 9.03 | 9.28 |
| $\delta^*$ | 0.128 | 0.127 | 0.124 | 0.130 |
| $\theta^*$ | 0.069 | 0.068 | 0.068 | 0.071 |
| $H$ | 1.85 | 1.86 | 1.83 | 1.83 |

*Note.* PIV and LDA are measurements from Westerweel *et al.*, DNS-E are results from Eggels *et al.* [2], and DNS-AM are the results from the present calculations.

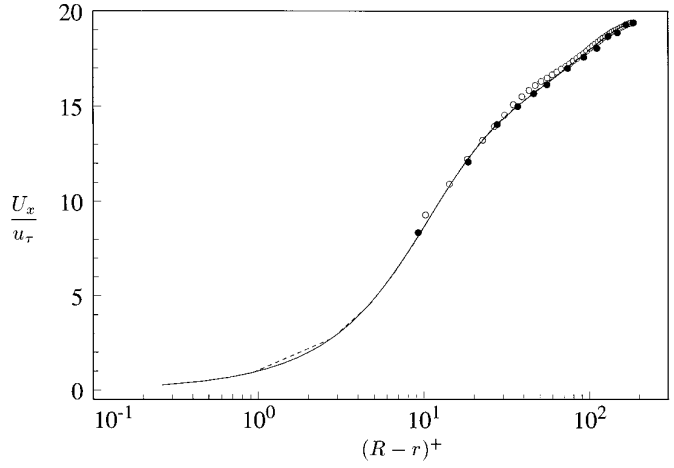


**FIG. 6.** Mean velocity profile: ———, DNS-AM; ---, DNS-E; ○, PIV, Westerweel *et al.*; ●, LDA, Westerweel *et al.*

on the bulk velocity, $U_b$, and calculated from the expression:

$$C_f = \tau_{\text{wall}}/\tfrac{1}{2}\rho U_b^2. \tag{15}$$

From Table II it follows that the present DNS results agree to within a few tenths of a percent with those of Eggels *et al.* [2]. Westerweel *et al.* [16] measured statistical quantities in turbulent pipe flow using laser Doppler anemometry (LDA) and particle image velocimetry (PIV). Table II shows good agreement also with the experimental results of Westerweel *et al.*

Figure 6 shows the mean velocity profiles plotted in wall coordinates. Excellent agreement between the present DNS result and the two reference cases is observed.

Turbulence intensities are shown in Fig. 7. An overall good agreement is observed between the present DNS case and the DNS results of Eggels *et al.* [2]. The somewhat high value of $u_x'$ around the peak in the profile from the PIV measurements of Westerweel *et al.* is regarded as a statistical error. Despite these problems the experimental values agree reasonably well with the DNS data.

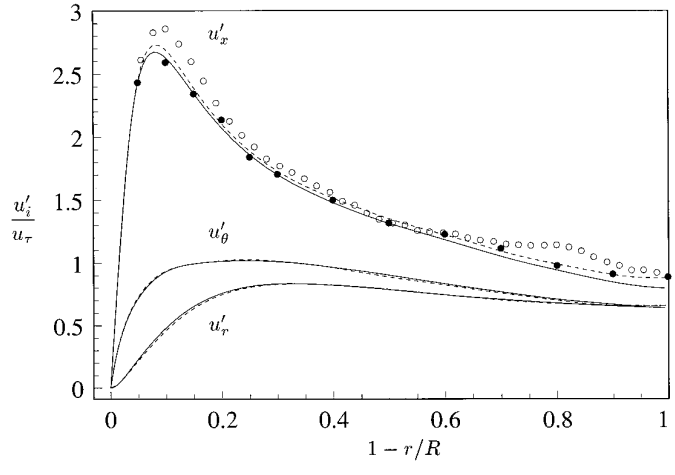


**FIG. 7.** Turbulence intensities: ———, DNS-AM; ---, DNS-E; ○, PIV, Westerweel *et al.*; ●, LDA, Westerweel *et al.*

## 8. COMPUTATIONAL COST

As pointed out previously, the time-integration method described in this paper divides the computational domain into two sections, treating different terms in each section with implicit or explicit time-integration schemes. The method used by Eggels *et al.* [2] addressed the problems related to the fine azimuthal grid resolution around the centerline by treating all terms with derivatives in the azimuthal direction implicitly. However, this leaves a trade-off between the minimum obtainable radial resolution and the maximum possible time-step. The radial grid-spacing used by Eggels *et al.* [2] was $\Delta r u_\tau/\nu = 1.88$; the maximum time-step, $\Delta t$, was then limited to $0.0004\ R/u_\tau$.

For comparison, the maximum time-step used in the present DNS calculation was $0.001\ R/u_\tau$ (a factor of 2.5 higher than that used by Eggels *et al.* [2]) with a minimum radial grid-spacing at the wall of $\Delta r^+ = 0.17$. This is a factor of 10 smaller than the radial grid-spacing used by Eggels *et al.* [2]. Since the maximum time-step goes as $\Delta r^2$, the radial resolution used in the present case could not have been used if only terms with derivatives in the azimuthal direction were treated implicitly.

Eggels *et al.* [2] report that their code needed about 5.7 CPU hours per non-dimensional time-unit on a Cray YMP. This would correspond to about 2.6 CPU hours on a Cray C-90. Due to the higher time-step used, the present DNS calculation required only about 1.3 CPU hours per nondimensional time-unit. The numerical scheme developed in this paper is therefore significantly less CPU time-consuming than the scheme used by Eggels *et al.* [2], yet it allows for more flexibility in terms of radial and azimuthal clustering of grid points.

To evaluate the CPU time savings of the new scheme, consider the following quantity which is related to the stability criterion if all terms are treated explicitly:

$$\text{SC} = \Delta t\left\{\frac{|u_x|}{\Delta x} + \frac{|u_r|}{\Delta r} + \frac{|u_\theta|}{r\,\Delta\theta} + 4\nu\left(\frac{1}{\Delta x^2} + \frac{1}{\Delta r^2} + \frac{1}{(r\,\Delta\theta)^2}\right)\right\}. \tag{16}$$

The first three terms on the right-hand side of Eq. (16) are related to the convective terms and the last three terms are due to the diffusive terms. The maximum of the terms

in Eq. (16) were calculated in the simulation described previously (DNS-AM), both in the core and in the outer region, yielding

$$
\begin{array}{lccc}
\mathrm{SC} = & \left\{ \dfrac{\Delta t|u_x|}{\Delta x} \right. & + \dfrac{\Delta t|u_r|}{\Delta r} & + \dfrac{\Delta t|u_\theta|}{r\,\Delta\theta} \\
\text{Core:} & 0.5 & 0.1 & 5.0 \\
\text{Outer:} & 0.5 & 0.6 & 0.1 \\
& + \dfrac{\Delta t 4\nu}{\Delta x^2} & + \dfrac{\Delta t 4\nu}{\Delta r^2} & \left. + \dfrac{\Delta t 4\nu}{(r\,\Delta\theta)^2} \right\} \\
& 1.5 \times 10^{-2} & 0.1 & 1.8 \times 10^{2} \\
& 1.5 \times 10^{-2} & 25.0 & 3.1 \times 10^{-2}\,.
\end{array}
$$

The stability limit for a fully explicit RK3 scheme is $SC \leq \sqrt{3}$. It is clear that both the convective and diffusive terms with derivatives in the azimuthal direction have to be treated implicitly in the core region in order to be able to maintain the time-step used in the simulation. If the convective terms (with derivatives in the azimuthal direction) were treated explicitly, the time-step would have to be reduced by a factor of $5/\sqrt{3}$ in order to maintain numerical stability. Treating the diffusive terms (with derivatives in the azimuthal direction) explicitly in the core region would reduce the maximum time-step by a factor of 100. Thus, it is clearly important to treat these terms implicitly. In the outer region it is seen that the diffusive terms (with derivatives in the radial direction) need to be treated implicitly in order to avoid significant time-step restrictions.

This analysis also shows why it makes little sense to treat all diffusive terms implicitly and all convective terms explicitly as proposed in [8]. First of all, there is no need to treat diffusive terms with derivative in the axial direction implicitly in any region of the flow. Since explicit schemes generally are simpler and less CPU intensive, they should be used whenever possible. Lastly, the analysis shows that in some cases it may be important to also treat convective terms implicitly in order to avoid significant time-step restrictions. Which terms to treat explicitly/implicitly should therefore be tailored to the specific problem at hand.

## 9. WHERE TO PLACE THE INTERFACE

In general the location of the interface is determined to maximize the time-step. The error estimate, described in Section 6, is generally not used to determine $r_c$ since the error in each region is determined by the temporal integration scheme used. However, the overall error may in some cases (see Sections 6 and 7) be reduced by moving the interface either towards the centerline or the pipe wall.

The general rule is to place the interface in a region where the grid is fairly coarse in all coordinate directions. For flow in a pipe this means away from the centerline and away from the wall. Fortunately it seems to be quite arbitrary where the interface is placed as long as regions with very fine grid is avoided. This is illustrated in Fig. 8, which shows the contribution to the stability criterion (SC) from each term in Eq. (16), plotted versus radial distance (for the case described in Section 7).

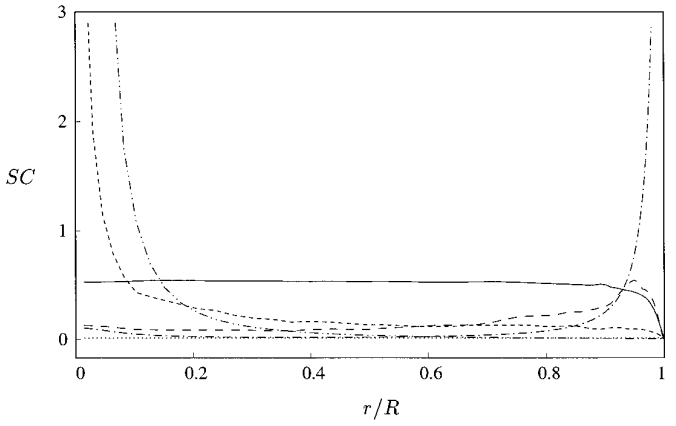


**FIG. 8.** The maximum of the terms in Eq. (16) plotted versus radial distance: ———, $\Delta t|u_x|/\Delta x$; – – –, $\Delta t|u_r|/\Delta r$; - - -, $\Delta t|u_\theta|/r\,\Delta\theta$; ···, $\Delta t 4\nu/\Delta x^2$; –·–, $\Delta t 4\nu/\Delta r^2$; –··–, $\Delta t 4\nu/(r\,\Delta\theta)^2$.

It is clear that the terms $\Delta t|u_\theta|/r\,\Delta\theta$ and $\Delta t 4\nu/(r\,\Delta\theta)^2$ impose severe time-step limitations close to the centerline. At the wall, the term $\Delta t 4\nu/\Delta r^2$ is seen to pose significant restrictions. However, there is a fairly wide range (from about $r/R = 0.15$ to $r/R = 0.9$), where all the terms in Eqs. (16) are small and of roughly the same order of magnitude. The interface, $r_c$, could be placed anywhere in this range without significantly affecting the maximum time-step allowed.

## 10. SUMMARY

A method has been developed for temporal integration of the Navier–Stokes equations formulated in cylindrical coordinates. One of the problems faced in cylindrical coordinates, particularly in confined axisymmetric geometries, is that in order to obtain sufficient azimuthal resolution at the wall, the azimuthal resolution in the core of the flow becomes unnecessarily fine, leading to significant time-step limitations if explicit time-integration schemes are used. At the same time it is desirable to maintain a fine radial resolution at the wall.

The method described in this paper divides the computational domain into two regions in which terms with derivatives in only one coordinate direction are treated implicitly. This leads to at most one nonlinear equation which can easily be linearized. The solution scheme is therefore much

simpler than if the entire computational domain was treated with one temporal integration scheme which in many cases would lead to a set of coupled nonlinear equations. Even though linearization could still be used, a large block tridiagonal matrix would have to be solved which would require the use of either an iterative technique or an approximate factorization scheme.

The new method has been implemented both in a code calculating turbulent flow in a cylindrical pipe and in a code used for the study of turbulent mixing in a coaxial jet-combustor (see [1]). DNS results from the pipe flow code compare favorably with computational and experimental results from the literature. In particular it was demonstrated that the new method allows for a 2.5 times increase in the maximum time-step, compared with the DNS code used by Eggels *et al.* [2] in which all terms with derivatives in the azimuthal direction were treated implicitly in the entire computational domain. Thinner boundary layers with higher Reynolds numbers would result in larger savings with the present method. In addition to a significant increase in time-step the new method allowed for a small radial grid-spacing at the wall, about 10 times smaller than that used by Eggels *et al.* [2].

## ACKNOWLEDGMENTS

This work was sponsored by a grant (F49620-92-J-003) from the Air Force Office of Scientific Research. Discussions with Dr. Thomas Lund are gratefully acknowledged.

## REFERENCES

1. K. Akselvoll and P. Moin, Report TF-63, Department of Mech. Eng., Stanford University, 1995.
2. J. G. M. Eggels, F. Unger, M. H. Weiss, J. Westerweel, R. J. Adrian, R. Friedrich, and F. T. M. Nieuwstadt, *J. Fluid Mech.* **268,** 175 (1994).
3. H. Weizhang and D. Sloan, *J. Comput. Phys.* **107,** 254 (1993).
4. M. D. Griffin, E. Jones, and J. D. Anderson, *J. Comput. Phys.* **30,** 352 (1979).
5. Y. Kurihara, *Mon. Weather Rev.* **93**(7), 399 (1965).
6. L. Umscheid and M. Sankar-Rao, *Mon. Weather Rev.* **99**(9), 686 (1971).
7. C. Wagner and R. Friedrich, "Direct Numerical Simulation of Turbulent Flow in a Sudden Pipe Expansion" in *AGARD Symposium on Application of Direct and Large-Eddy Simulation to Transition and Turbulence. April 18–21, Chania, Crete, Greece, 1994.*
8. J. Kim and P. Moin, *J. Comput. Phys.* **59**(2), 308 (1985).
9. J. M. Oberhuber, *J. Phys. Oceanogr.* **23,** 808 (1993).
10. M. Kwizak and J. A. Robert, *Mon. Weather Rev.* **99**(1), 32 (1971).
11. P. R. Spalart, Internal Report, NASA-Ames Research Center, Moffett Field, CA., 1987 (unpublished).
12. P. R. Spalart, R. D. Moser, and M. M. Rogers, *J. Comput. Phys.* **96,** 297 (1991).
13. J. B. Perot, *J. Comput. Phys.* **108**(1), 51 (1993).
14. J. K. Dukowicz, and A. S. Dvinsky, *J. Comput. Phys.* **102**(2), 336 (1992).
15. F. H. Harlow and J. E. Welch, *Phys. Fluids* **8**(12), 2182 (1965).
16. J. Westerweel, R. J. Adrian, J. G. M. Eggels, F. T. M. Nieuwstadt, "Measurements with Particle Image Velocimetry on Fully Developed Turbulent Pipe Flow at Low Reynolds Number," *Proceedings, 6th Int. Symp. on Appl. of Laser Technol. to Fluid Mech., Lisbon, Portugal, July 20–23, 1992*
17. H. Le and P. Moin, *J. Comput. Phys.* **92**(2), 369 (1991).